RSC Advances

ROYAL SOCIETY OF CHEMISTRY

www.rsc.org/advances

$CdS:SiO_2$ nanocomposite as luminescence based wide range temperature sensor

Nupur Saxena*, Pragati Kumar, and Vinay Gupta

Department of Physics & Astrophysics, University of Delhi, Delhi-110 007, India

*E-mail: n1saxena@gmail.com

Authors

Nupur Saxena (Corresponding Author)
Department of Physics & Astrophysics,
University of Delhi-110007, India
Phone No.: +91 11-27667036,
Fax No.: +91 11-27667036
E-mail: n1saxena@gmail.com

Pragati Kumar,
Department of Physics & Astrophysics,
University of Delhi-110007, India

Vinay Gupta
Department of Physics & Astrophysics
University of Delhi, Delhi-110 007, India,

Abstract

A wide range (20-560K) temperature sensor is devised for the first time from $CdS:SiO_2$ nanocomposite thin films grown by pulsed laser deposition. Highly intense, stable, and broad red emission observed from $CdS:SiO_2$ nanocomposite is employed to achieve the luminescence thermometer. Nearly monodispersity and small size of CdS nanocrystals (~ 3 nm) in SiO_2 matrix as viewed by transmission electron microscope may be accountable for the absence of band edge emission even at 20 K. The sensor exhibits almost linear behavior in all cryogenic, physiological, and high temperature ranges. The average sensitivity and resolution of the sensor reported here are $\approx 10^{-2}$ K^{-1} and 10^{-4} K respectively with a maximum relative sensitivity ~ 8.4 % K^{-1} at 120 K.

Keywords: $CdS:SiO_2$ nanocomposite, Pulsed laser deposition, Photoluminescence, Temperature sensor.

1. Introduction

Temperature is a fundamental thermodynamic quantity, measurement of which is crucial for wide range of applications and in diverse areas from biological sciences to space sciences. Thermometry has been carried out employing various properties of materials including change in resistance, thermal expansion of solid or liquid, change in pressure of a gas or measurement of infrared energy emitted by an object in radiation type thermometers. Among all these only radiation type thermometers operates in non-contact mode. To realize the temperature measurement in micro/nano scale with high resolution and sensitivity, luminescence thermometry is most widely applicable.

Optical temperature sensors are important in many thermometry applications as they provide immunity to electrical noises, better sensitivity, selectivity, and fast response. A variety of devices has been reported utilizing optical fiber sensing[1], surface plasmon resonance method (change in dielectric constant, refractive index)[2], photoluminescence (change in intensity, peak position, lifetime)[3-7], shift in optical absorption edge[8] etc. to realize optical thermometers in different ranges. Particularly, photoluminescence (PL) based temperature sensors are widely applicable because of their low-cost, simple preparation, easy instrumentation, noninvasive operation, and nondestructive technique for detection of temperature even for living or cancer cells[4]. It is observed that PL intensity or luminescence intensity ratio (LIR) is such a parameter that can offer versatility for sensing different environments as compared to other techniques[9]. This ability to glean the temperature is demonstrated by certain luminescent materials including II-VI semiconductors quantum dots (QDs)[6,7,10-14], carbon dots[15], lanthanide based complexes[1,3,16-18], metal-organic-frameworks (MOFs)[5,19] etc. Among these II-VI semiconductors (especially Cd-containing QDs) and their nanocomposites are used outstandingly. In the report by Walker et. al.

a luminescence intensity based thermometer was realized by CdSe QDs with a ZnS overlayer [(CdSe)ZnS] in poly(lauryl methacrylate) (PLMA) matrix in the temperature range 100 to 315 K and observed a relative sensitivity of 1.3% per °C[6]. P. A. S . Jorge et. al. devised (CdSe)ZnS core-shell doped bulk glass temperature sensor (287 – 316K) with a resolution of 0.3 °C and for intensity based sensing and sensitivity of 0.2 nm $°C^{-1}$ for wavelength shift based sensing[7]. Local temperature sensing (297.4 – 316.6 K) using single QDs of (CdSe)ZnS coated with a layer of organic polymer, and conjugated with streptavidin was carried out by S. Li and co-workers and achieved a sensitivity of ~ 0.1 nm/°C using PL spectral shift[10]. A CdSe(ZnS):SiO_2 nanocomposite based high temperature sensor (295-525K) is demonstrated. The optical thermometer worked on the variation of the emission wavelength with temperature and exhibited a sensitivity of ~ 0.11 nm$°C^{-1}$. The core-shell structure of CdSe(ZnS) QDs with E_{CdSe} = 2.04 eV and E_{ZnS} = 2.72 eV encapsulated with SiO_2 is employed to obtain high yield and intense emission in visible range[11]. Maestro et. al. demonstrated the potential use of CdSe QDs as fluorescent nanothermometers for two-photon fluorescence microscopy. This nanothermometer displayed not just enhancement in spatial resolution for multiphoton excitation processes, rather higher temperature sensitivity for two-photon (near-infrared) excitation as compared to that under one-photon (visible) excitation. Additionally, the peak emission wavelength was also found to be temperature sensitive[12]. A temperature sensor (296 – 353 K) based on ultrathin film system of mercaptosuccinic acid modified CdTe QDs and positively charged layered double hydroxide nanosheets with high response sensitivity (1.47% per °C) is reported by R. Liang et. al. recently[13]. However, mostly Cd-containing QDs based temperature sensors suffer limited temperature variation, poor sensitivity and thermal stability. Hence, it is a challenge to devise new types of QDs based temperature sensors with wide range of temperature, thermal stability,

reproducibility, and better sensitivity.

In this article, we report a simple and low-cost CdS:SiO_2 nanocomposite system which is chemically pure, thermally stable and offers a broad red luminescence that opens new channels for futuristic photonic, optoelectronic and sensing devices. Particularly, this work is dedicated to fabricate a versatile range temperature sensor based on emission from this system. CdS is a direct band gap (for bulk CdS E_g = 2.42 eV) II-VIth semiconductor that exhibits tunable optical properties and emission cover full range of visible spectrum. Due to this property, CdS QDs are extensively used in diverse applications including photodetection[20], light-emitting diodes[21], solar cells[22], lasers[23], waveguide[24], bio-imaging[25], and photoelectrochemical sensors[26]. An optically transparent matrix such as SiO_2 provides multifold recompenses like stabilization of emission, prevention from contaminations and oxidation that can affect the emission extensively[11]. Encapsulation of CdS with SiO_2 in the form of nanocomposite provides this system thermal resistance, transparency, stability, and multifold enhancement in emission intensity. The intense room temperature luminescence from CdS:SiO_2 nanocomposite motivates for future research towards diverse applications of this system. A wide range luminescence based thermometer realized out of it is just a step for harnessing the extraordinary emission properties of this composite system.

2. Experimental details

2.1 CdS QDs and target preparation

CdS QDs were synthesized by chemical co-precipitation method using $Cd(NO_3)_2$ and Na_2S as precursors procured from Sigma Aldrich Ltd. (USA). The detailed report on the synthesis and characterization of CdS QDs is published elsewhere[27]. The target for laser ablation of CdS QDs

was prepared by pressing and sintering the CdS QDs powder while the target of SiO_2 is purchased from Sigma Aldrich Ltd. (USA).

2.2 Sensor fabrication

The nanocomposite thin films are grown by pulsed laser deposition (PLD) using target swapping method followed by thermal annealing at 400 and 500 °C in Ar ambience for 3 hrs to obtain crystalline phase of CdS. The swapping frequency is the key parameter to decide the final composition of the nanocomposite system. An Nd:YAG laser (Continuum) operating in 3rd harmonic mode with wavelength λ = 355 nm is directed towards the rotating target of CdS and SiO_2 for deposition of CdS and SiO_2 in the form of layer by layer on n-type (110) silicon substrate and carbon coated Cu grids for transmission electron microscopy (TEM) imaging. Before ablation of the targets, the stainless steel chamber was evacuated to 5E-6 mbar. The energy of the laser beam is kept 200 mJ, repetition rate and pulse width as 10 Hz and 10 ns respectively for this experiment. The details of sample preparation method and structural confirmation by x-ray photoelectron spectroscopy, glancing angle x-ray diffraction, and Raman spectroscopy is discussed elsewhere[28].

2.3 Sensor Characterizations

Bright field TEM (BFTEM) imaging of the nanocomposites is carried out using Tecnai G20-stwin microscope operating at 300 kV equipped with LaB_6 filament and a charge-coupled device camera having a point resolution of 1.44 Å and line resolution of 2.32 Å. Photoluminescence (PL) spectroscopy studies are carried out in temperature range 20K – 560K using Jobin Yvon Triax 550 monochromator combined with a liquid-nitrogen cooled InGaAs detector of resolution $\approx 10^{-5}$. The samples are excited with 325 nm wavelength of He-Cd laser.

3. Results and Discussion

The room temperature PL (RTPL) of as grown, annealed at 400 °C and 500 °C nanocomposites are shown in Fig. 1. The RTPL inherits an emission peak centered at ~ 630 nm with a small hump at ~ 605 nm for as grown nanocomposite both related to red emission (RE) without any sign of band edge emission. Dib et al. suggested that the band-edge PL band (~ 515 nm for bulk CdS) appears due to the direct excitonic recombination in quantum dots (QDs) having a diameter larger than 3 nm. The other QDs (the majority), are either non-luminescent due to non-radiative processes, or luminescent at higher wavelength by recombination of the trapped charge carriers because in the strong confinement the only allowed transition is from singlet states and other transitions are forbidden[29]. Thus, absence of band edge emission indicates that the dominating process in present study is surface state recombination and may be attributed to very narrow distribution with large number of small nanocrystals[30]. The similar feature is well visualized in TEM micrographs as discussed elsewhere in detail[28]. It is well established now that the origin of trap emission occurs because of the high amount of surface defects, site-substitutional impurities, or vacancies[30]. The RE from CdS is originated from the transition of bound electrons from surface states to the valence band (VB)[28,31]. The defects responsible for such transitions are sulfur vacancies (V_S^{2+})[31,32] or cadmium vacancies (V_{Cd}^{2-})[31,33].

Thermal annealing of nanocomposite causes enhancement in emission intensity with a maximum shift of ~ 15 nm in peak position towards higher wavelength. The enhancement in intensity by annealing may be resulted by alteration of interface conditions of CdS QDs and SiO_2 matrix in the nanocomposite i.e. coalescence of very tiny particles thereby improving the crystallinity and formation of large amount of surface defects such as cadmium and sulphur vacancies due to ionic displacements during recrystallization[34,35]. The communal effects accountable for the observed intense RE in nanocomposites are the interaction of CdS

nanoparticles with SiO_2 matrix at their interfaces and thermal annealing. In the present study, the temperature sensing is performed only on the nanocomposite annealed at 500 °C because of its highest emission intensity.

BFTEM studies envisage the formation of almost mono-dispersed CdS nanoparticles of ~ 3 nm in SiO_2 matrix after annealing at 500 °C as shown in Fig.2. The average inter-particle separation is ~ 12 nm, which is crucial in order to get high intense and pure emission. The inset shows particle size distribution histogram, which indicates that, size of the CdS nanoparticles ranges from 1.5 to 6 nm. The lognormal fitting to the histogram suggests the average particle size as 3.0 ± 0.2 nm predicting almost monodispersity in the nanocomposite system. Selected area electron diffraction (SAED) pattern confirms the hexagonal phase of CdS with d-spacings as 3.54 Å, 3.34 Å and 3.12 Å corresponding to (100), (002) and (101) crystal orientations (Inset Fig.2.).

The stability of PL intensity at RT for present sensor is also studied with respect to time and shown in Fig.3. It is clear that the intensity remains almost unchanged in due course of time. For better visualization, the upper part of the spectra is shown in zoom. It is illustrated that the rate of intensity reduction for first six months is relatively larger than later and almost saturates after two years (Inset Fig.3). It is significant to note that even after two or more years, the PL intensity is preserved to 95% of its initial value.

The evolution of RE intensity with lowering of temperature is shown in Fig.4a. The emission intensity enhances gradually, as the temperature is lowered upto 20 K. This enhancement in intensity is usual due to the thermal deactivation of non-radiative transitions[36]. The spectra do not show evolution of any new peak even at 20 K, implies that the only possible traps that contributes in emission are either due to sulfur vacancies (V_S^{2+}) or cadmium vacancies

(V_{Cd}^{2-}) or both. The shifting in peak position is marginal being maximum upto 15 nm at 20 K stating a high stability in the trap emission in lower temperature range. It is observed that at RT, emission intensity is high enough to study temperature dependency of emission spectra above RT. The stagnation of PL intensity is observed with rising temperature and is shown in Fig.4b. The peak shift is relatively more (~ 35 nm) in this case as compared to lower temperature side, but still trivial. Hence, the emission is considerably stable in both the temperature regions. The data is taken in reversible and repetitive manner to check the repeatability and reliability. This behavior of PL gears-up to be utilized as a probe for temperature.

Fig. 5 depicts the linear behavior of the temperature sensor studied as a function of inverse temperature according to the linear function $ln\ P = -\frac{\varepsilon}{kT} + lnA$, deduced from the variation of integrated intensity with respect to temperature according to[30]:

$$I_T = \frac{B}{Ae^{-\varepsilon/kT}+1} \quad (1)$$

where, A and B are constants, ε is the activation energy, k is the Boltzmann constant and $P = \frac{I_T}{B} - 1$. The variation of integrated intensity is plotted as a function of temperature and shown in inset of Fig. 5. The constants are determined by fitting the experimental data with above mentioned equation and are found as $A = 42.7, B = 2565282\ and\ \varepsilon = 0.043\ eV$. The linear behavior of the intensity with inverse of temperature suggests its potential application in temperature sensor. For clarity, the linear behavior of temperature sensor above RT is shown separately in Fig. 5 (inset).

The sensor response is also studied in terms of PL spectrum full width at half maximum (FWHM) and is plotted as a function of temperature shown in Fig. 6. Whereas intensity gives a direct interpretation of temperature, FWHM is analytical. The collective effect of homogeneous and inhomogeneous broadening results in the increase in FWHM of PL spectrum with rise in

temperature. The underlying reasons for such broadenings are: (i) broad distribution of intraband states caused by different trapping sites, (ii) distribution in trapped e-h distances (iii) carrier-phonon interactions due to scattering of excitons with acoustic and longitudinal optical (LO) phonons and (iv) nanocrystallites size distribution induced inhomogeneous broadening. For the broadening of PL spectrum is mainly originated by (iii) and (iv) sources significantly. The third one causes homogeneous broadening while fourth is responsible for inhomogeneous broadening in the PL spectrum due to thermal treatment. The solid curve is obtained using modified Toyozawa's equation[37] which is stated as:

$$FWHM(T) = \frac{A}{(e^{E_{LO}/k_B T}-1)} + BT + C \qquad (2)$$

where, A is the temperature independent linewidth parameter for the exciton-LO phonon-coupling strength; E_{LO} is the LO-phonon energy for the fundamental mode in Raman spectrum of CdS QDs taken as 37.2 meV; B is the exciton-acoustic phonon coupling coefficient; C is the inhomogeneous broadening, which is temperature-independent and it is due to distribution in size, shape, composition of the nanocrystals. The other parameters obtained by fitting the above equation to FWHM are listed in table as shown in inset of Fig. 6. The exciton-LO phonon-coupling coefficient is smaller than that of about 180.6 meV in single crystal CdS due to the confinement of excitonic polarization in small QDs in nanocomposite system.

Temperature sensing in the cryogenic, physiological, and high temperature range has been studied with various materials. Nevertheless, there is rarely any report on such a wide range temperature sensor using inorganic compounds and simple fabrication processes. The efficiency of the temperature sensor reported here can be quantified as high sensitivity and resolution. The sensitivity of the sensor is related to the slope of the linear fit and defines the rate of change of intensity/FWHM with respect to the change in temperature. The average sensitivity of the sensor

in two temperature ranges is calculated using the relation $\Delta I/\Delta T$, where ΔI is the change in *ln P/FWHM* corresponding to change in temperature ΔT[38]. The resolution of the sensor is deduced from detector resolution and calculated sensitivity. The sensitivity of the sensor deduced from intensity studies is plotted with temperature and shown in Fig. 7. The sensitivity decreases with increasing the temperature due to the drastic change in emission intensity at lower temperature regime and stability at higher temperatures. The calculated sensitivity and resolution in the two temperature ranges are given in inset of Fig. 7. The average sensitivity and resolution of the sensor are calculated as ~ 0.06 K^{-1} and 0.0002 K respectively for intensity while ~ 0.389 meV K^{-1} for FWHM measurements. The relative sensitivity of the sensor[38] i.e.

$$R_s(T) = \left|\frac{1}{P}\frac{dP}{dT}\right| \quad (3)$$

reaches as high as ~ 8.4 % K^{-1} at 120 K (shown in Fig. 7) while better resolution ~ 0.003 K is observed in high temperature regime.

A brief review on the luminescence based thermometers is presented in Table 1 for comparison. It includes work on diverse range of materials to realize nanothermometers of high sensitivity. In most of the studies, luminescence intensity ratio in rare earth doped compounds/complexes or alternatively PL intensity/spectral shift in Cd-containing QDs are studied with respect to temperature. Particularly, for Cd-containing QDs temperature sensors, the sensitivity is not very satisfactory, maximum being 1.47% $°C^{-1}$ for CdTe quantum dots–layered double hydroxide ultrathin films[13] with limited range of temperature response. Some sensors are useful in cryogenic temperatures, some in physiological while others are good for high temperature range. Nevertheless, such wide range temperature sensor that covers all temperature zones is not yet reported. The sensitivity and resolution of the present sensor is considerably better in all temperature regimes in case of intensity study. The study of luminescence intensity

with temperature for present sensor is a direct and significant method as compared to the other ones due to single peak observed in PL spectrum. The advantage here is that the temperature can be sensed directly by observation of lowering or evolution of intensity of PL spectrum. Usually in most of temperature sensors like rare earth doped complexes, there are two sharp peaks for which the intensity ratio varies with temperature and a direct linear or natural log based linear relation can be obtained for temperature sensor. Instead, for CdS:SiO_2 nanocomposite temperature sensor, there is no need to observe the ratio of PL peaks which is not easy to perceive. We have also performed FWHM studies as a function of temperature and found that the sensor works with better sensitivity for luminescence intensity. The highest value of relative sensitivity (~ 8.4 $\%K^{-1}$) is maximum, being 1.2 times greater than the maximum achieved sensitivity so far[18] for luminescence based molecular thermometers. The present temperature sensor is a good choice in cryogenic region for better sensitivity whereas in high temperature zones for better resolution.

4. Conclusion:

In summary, a low-cost, highly efficient, sensitive and stable wide range temperature sensor using CdS:SiO_2 nanocomposite is reported here first time. The emission intensity and thereby the performance of the device is unprecedented even after a long time. The possible mechanism of pure, intense, and stable RE is discussed by considering the role of surface defects, monodispersion of CdS nanocrystals and SiO_2 matrix. The linearity of sensor is visualized in variation of *ln P* with inverse of temperature as $ln\ P = -((506.96 \pm 10)/T) + (3.74 \pm 0.07)$. The average sensitivity and resolution of the temperature sensor are ~ 0.06 K^{-1} and 0.0002 K respectively. The maximum relative sensitivity of 8.4 % K^{-1} is observed at 120 K.

Alternatively FWHM gives an analytic sensitivity of ~ 0.388 meV K^{-1} for this sensor. The achieved range, sensitivity, and resolution are far ahead of earlier reports.

Acknowledgements:

The authors (NS:F.13-905/2013(BSR) & PK:F.4-2/2006(BSR)/PH/13-14/0055) are thankful to University Grant Commission (UGC), India for providing Dr. D. S. Kothari post doctoral fellowship. The help received from Mr. Kun Gao HZDR, Germany in TDPL measurements is highly appreciated.

References:

1. C. D. S. Brites, P. P. Lima, N. J. O. Silva, A. Millán, V. S. Amaral, F. Palacio, and L. D. Carlos, *Adv. Mater.* 2010, 22, 4499.
2. S. Saha, N. Mehan, K. Sreenivas, and V. Gupta, *Appl. Phys. Lett.* 2009, 95, 071106.
3. M. G. Nikolic, Z. Antic, S. Culubrk, J. M. Nedeljkovic, M. D. Dramicanin, *Sensors and Actuators B* 2014, 201, 46.
4. F. Vetrone, R. Naccache, A. Zamarron, A. J. de la Fuente, F. Sanz-Rodriguez, L. M. Maestro, E. M. Rodriguez, D. Jaque, J. G. Sole, and J. A. Capobianco, *ACS Nano* 2010, 4 (6) 3254.
5. Y. Cui, H. Xu, Y. Yue, Z. Guo, J. Yu, Z. Chen, J. Gao, Y. Yang, G. Qian, and B. Chen, *J. Am. Chem. Soc.* 2012, 134, 3979.
6. G. W. Walker, V. C. Sundar, C. M. Rudzinski, A. W. Wun, M. G. Bawendi, and D. G. Nocera, *Appl. Phys. Lett.* 2003, 83, 3555.
7. P. A. S. Jorge, M. Mayeh, R. Benrashid, P. Caldas, J. L. Santos, and F. Farahi, *Meas. Sci. Technol.* 2006, 17, 1032.

8. K. Kyuma, S. Tai, T. Sawada, and M. Nunoshita, *IEEE Trans. Micro. Theory & Tech.*1982, MTT-30 (4), 522.
9. X. Wang, O. S. Wolfbeis, and R. J. Meier, *Chem. Soc. Rev.* 2013, 42, 7834.
10. S. Li, K. Zhang, J. M. Yang, L. Lin, and H. Yang, *Nano Lett.* 2007, 7(10), 3102.
11. D. Pugh-Thomas, B. M. Walsh, and M. C. Gupta, *Nanotechnology* 2011, 22, 185503.
12. L. M. Maestro, E. M. Rodríguez, F. S. Rodríguez, M. C. Iglesias-de la Cruz, A. Juarranz, R. Naccache, F. Vetrone, D. Jaque, J. A. Capobianco, and J. G. Sole, *Nano Lett.* 2010, 10, 5109.
13. R. Liang, R. Tian, W. Shi, Z. Liu, D. Yan, M. Wei, D. G. Evans and X. Duan, *Chem. Commun.*, 2013, 49, 969.
14. T. Pustelny, *Sensors and Actuators A,*1995, 49, 57.
15. C. Wang, Z. Xu, H. Cheng, H. Lin, M. G. Humphrey, and C. Zhang, *Carbon* 2015, 82, 87.
16. N. Rakov, and G. S. Maciel, *Optical Materials,* 2014, 37, 635.
17. M. A. R. C. Alencar, G. S. Maciel, C. B. de Araújo, and A. Patra, *Appl. Phys. Lett.* 2004, 84, 4753.
18. S. Huang, X. Wei, Y. Chen, and M. Yin, *J. Lum.* 2014, 152, 148.
19. Y. Han, C. Tian, Q. Li, and S. Du, *J. Mater. Chem. C* 2014, 2, 8065.
20. K. Deng, and L. Li, *Adv. Mater.* 2014, 26 2619.
21. S. Nizamoglu, E. Mutlugun, O. Akyuz1, N. K. Perkgoz1, H. V. Demir, L. Liebscher, S. Sapra, N. Gaponik, and A. Eychmuller, *New J. Phys.* 2008, 10, 023026.
22. Y. J. Shen and Y. L. Lee, *Nanotechnology*, 2008, 19, 045602.

23. L. Zhang, K. Wang, Z. Liu, G. Yang, G. Shen and Peixiang Lu, *Appl. Phys. Lett.* 2013, 102, 211915.

24. A. Pan, D. Liu, R. Liu, F. Wang, X. Zhau, and B. Zou, *Small,* 2005, 1, 980.

25. G. Jie, B. Liu, H. Pan, J. Zhu and H. Y. Chen, *Anal. Chem.* 2007, 79, 5574.

26. X. Li, C. Hu, Z. Zhao, K. Zhang and H. Liu, *Sensors and Actuators B* 2013, 182, 461.

27. P. Kumar, N. Saxena, F. Singh and A. Agarwal, *Physica B:Condensed Matter*, 2012, 407, 3347.

28. P. Kumar, N. Saxena, Apoorva, A. Agarwal, and V. Gupta, *Mater. Res. Bull.,* submitted.

29. M. Dib, M. Chamarro, V. Voliotis, J. L. Fave, C. Guenaud, P. Roussignol, T. Gacoin, J. P. Boilot, C. Delerue, G. Allan, and M. Lannoo, *Phys. Stat. Sol (b)* 1999, 212, 293.

30. S. Santhi, E. Bernstein, and F. Paille, *J. Lum.* 2006, 117, 101.

31. P. Kumar, N. Saxena, V. Gupta, F. Singh, and A. Agarwal, *J. Appl. Phys.* 2014, 116, 043517.

32. A. Palafox, G. R. Paredes, A. Maldonando, R. Asomoza, D. R. Acosta, and J. P. Gomez, *Sol. Energy Mat. Sol. Cells,* 1998, 55, 31.

33. P. Roy and S. K. Srivastava, *J. Phys. D: Appl. Phys.,* 2006, 39, 4771.

34. Y. J. Lin, C. F. You, H. C. Chang, C. J. Liu and C. A. Wu, *J. Lum.,* 2015, 158, 407.

35. P. Kumar, N. Saxena, R. Chandra, V. Gupta , A. Agarwal, and D. Kanjilal, *Nanoscale Research Letters,* 2012, 7,584.

36. L. Boetter-Jensen, S. W.S. McKeever, A. G. Wintle, *Optically Stimulated Luminescence Dosimetry*, Elsevier, Amsterdam, The Netherlands, 2003.

37. Y. Toyozawa, *Prog. Theor. Phys.* 1962, 27, 89.

38. E. J. McLaurin, L. R. Bradshaw, and D. R. Gamelin, *Chem. Mater.* 2013, 25, 1283.

Table Caption:

Table 1. Brief summary of performances of luminescence based temperature sensors.

Figure Captions:

FIG. 1. Room temperature photoluminescence of as-grown CdS:SiO_2 nanocomposite system alongwith annealed at 400 °C and 500 °C.

FIG. 2. TEM image of CdS:SiO_2 nanocomposite temperature sensor. Inset shows particle size histogram and SAED pattern.

FIG. 3. Room temperature photoluminescence of CdS:SiO_2 nanocomposite temperature sensor recorded at various course of time. Inset Intensity variation as a function of aging time.

FIG. 4. Temperature dependent PL of CdS:SiO_2 nanocomposite temperature sensor (a) below RT, and (b) above RT.

FIG. 5. Linear fitting to intensity as a function of inverse temperature as $\ln\left(\frac{I_T}{B}-1\right)=-\frac{\varepsilon}{kT}+lnA$. Inset variation of integrate intensity with rise in temperature. The linear fit to the experimental data is shown by red line.

FIG. 6. FWHM dependency on temperature. Solid curve represents fitting to the experimental data according to the eqn.2.

FIG. 7. Variation of absolute and relative sensitivities as a function of temperature. Inset: table of sensor parameters in two temperature regimes.

Table 1. Brief summary of performances of luminescence based temperature sensors.

Sensing Material	Temperature sensing method	Temp. Range	Absolute/Relative Sensitivity	Ref.
Rare earth element doped γ -Fe_2O_3 @TEOS/APTES NPs	Luminescence intensity ratio	10K-350K	0.5% K^{-1}	[1]
Eu^{3+} doped TiO_2 NPs	Florescence intensity ratio & life time	307K-533K	0.17 -2.43% K^{-1}	[3]
Mixed-Lanthanide MOF	Luminescence intensity ratio	10K-300K	…	[5]
(CdSe)ZnS QDs in PLMA	Luminescence intensity	100K-315K	1.3% $°C^{-1}$	[6]
(CdSe)ZnS QDs doped bulk glass	PL spectral shift	287K – 316K	0.2 nm $◦C^{-1}$	[7]
Single QDs of (CdSe)ZnS	PL spectral shift	297.4K – 316.6 K	0.1 nm $°C^{-1}$	[10]
CdSe(ZnS) nanocomposite	PL spectral shift	295K-525K	0.11 nm $°C^{-1}$	[11]
CdSe QDs	Luminescence intensity and spectral shift	303K-333K	0.16 nm $°C^{-1}$	[12]
CdTe quantum dots–layered double hydroxide ultrathin films	Luminescence intensity	296K–353K	1.47% $°C^{-1}$	[13]
(ZnCd)S:Ag powder	Luminescence decay time	263K-423K	…	[14]
Carbon dots	Luminescence intensity	288K-333K	…	[15]
Tb^{3+} doped crystalline oxide powders	Luminescence intensity ratio	303K-773K	2.8×10^{-4} to $9\times10^{-4}°C^{-1}$	[16]
Er^{3+} doped $BaTiO_3$ NCs	Fluorescence intensity ratio	322K-466K	≤0.0052 K^{-1}	[17]
Eu^{3+} doped Y_2MoO_6	Luminescence intensity	20K-500K	7% K^{-1}	[18]
$Eu_xTb_{(1-x)}$MOF	Luminescence intensity ratio	100K-450K	1.325% K^{-1}	[19]
CdS:SiO_2 nanocomposite	Luminescence intensity & FWHM	20K-560K	Intensity: 0.006 K^{-1}/ 8.4% K^{-1} FWHM:0.388 meV K^{-1}	Present work

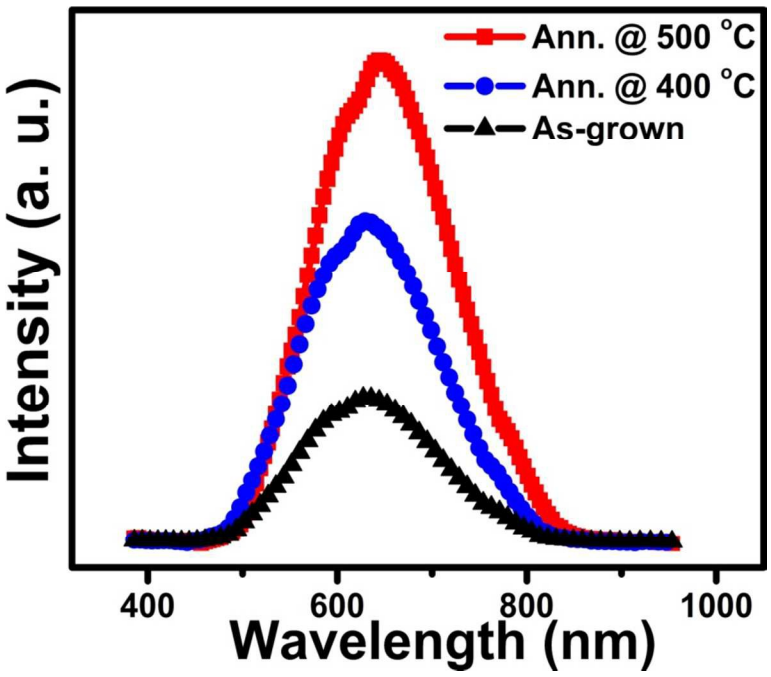

FIG. 1. Room temperature photoluminescence of as-grown CdS:SiO_2 nanocomposite system alongwith annealed at 400 °C and 500 °C.

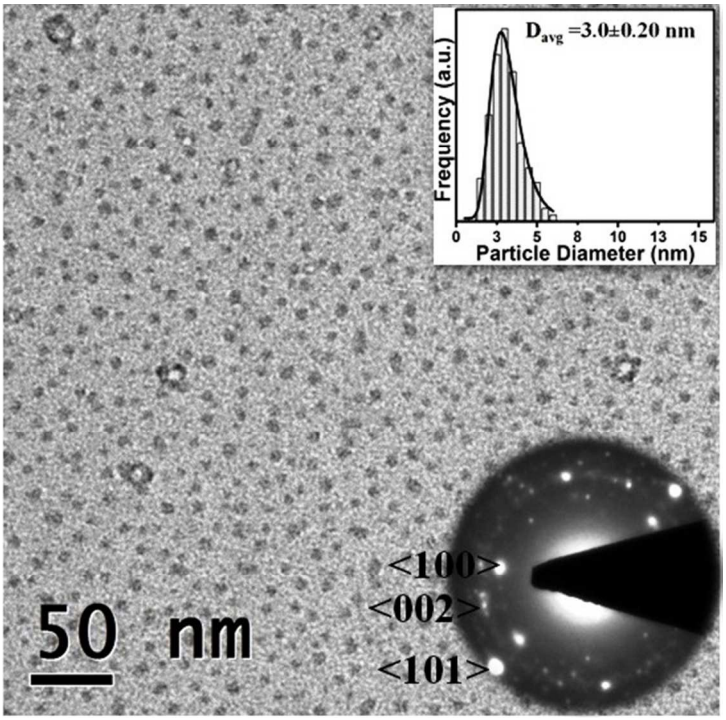

FIG. 2. TEM image of CdS:SiO_2 nanocomposite temperature sensor. Inset shows particle size histogram and SAED pattern.

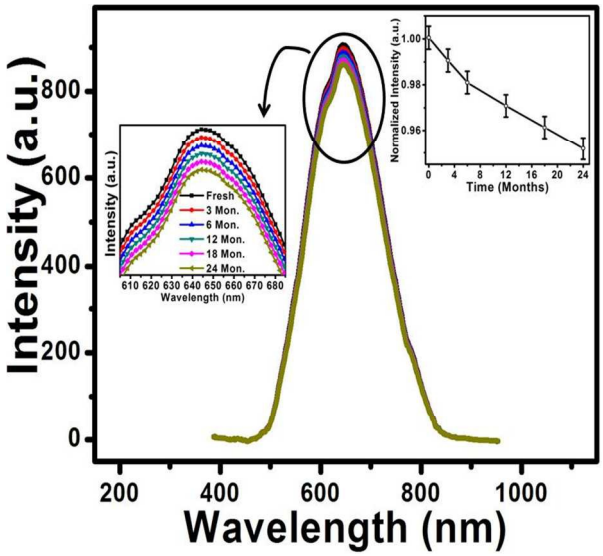

FIG. 3. Room temperature photoluminescence of CdS:SiO_2 nanocomposite temperature sensor recorded at various course of time. Inset Intensity variation as a function of aging time.

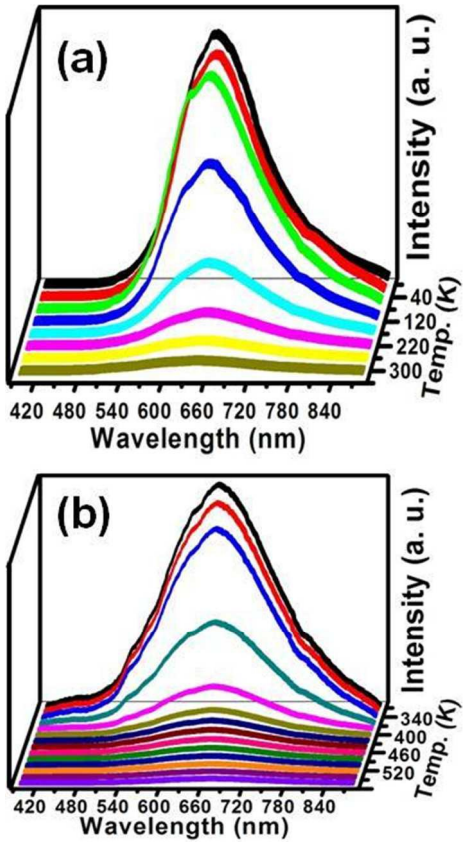

FIG. 4. Temperature dependent PL of CdS:SiO_2 nanocomposite temperature sensor (a) below RT, and (b) above RT.

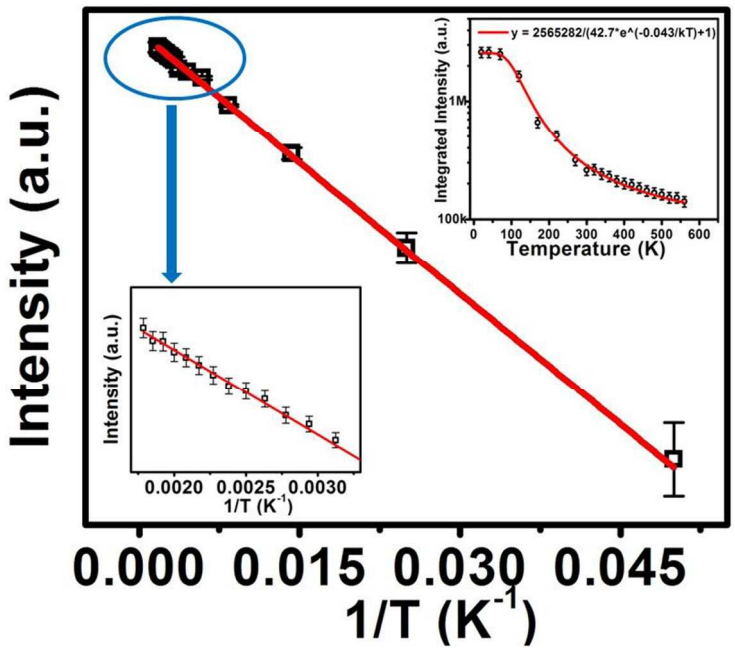

FIG. 5. Linear fitting to intensity as a function of inverse temperature as $ln\left(\frac{I_T}{B}-1\right)=-\frac{\varepsilon}{kT}+lnA$. Inset variation of integrate intensity with rise in temperature. The linear fit to the experimental data is shown by red line.

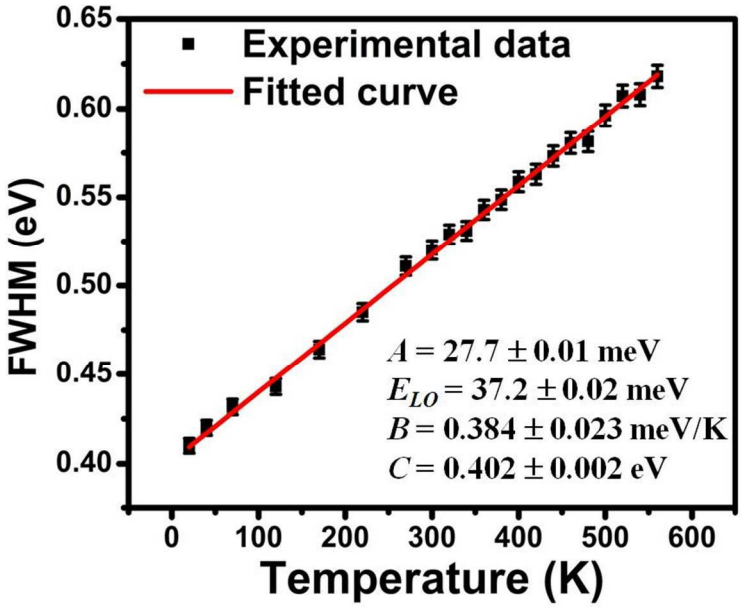

FIG. 6. FWHM dependency on temperature. Solid curve represents fitting to the experimental data according to the eqn.2.

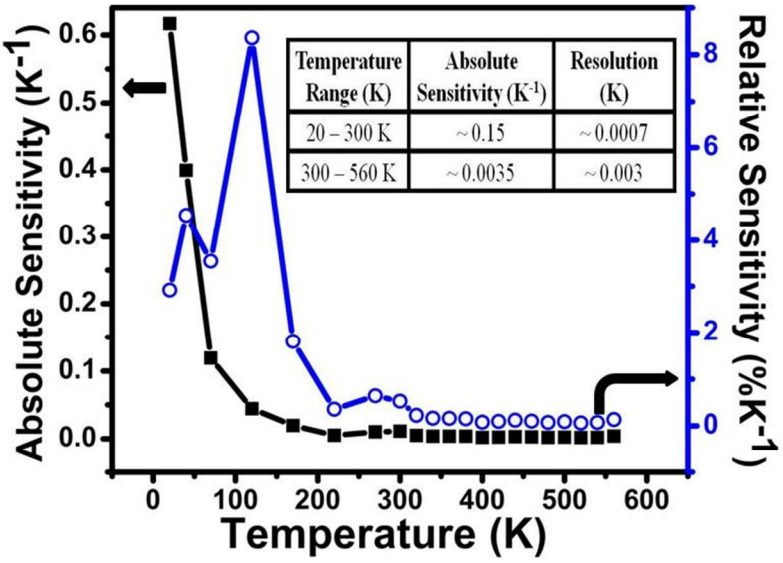

FIG. 7. Variation of sensitivity as a function of temperature. Inset table of sensor parameters in two temperature regimes.